Wisep j060738.65+242953.4: A Nearby Pole-on L8 Brown Dwarf With Radio Emission

The Harvard community has made this article openly available. Please share how this access benefits you. Your story matters

Citation	Gizis, John E., Peter K. G. Williams, Adam J. Burgasser, Mattia Libralato, Domenico Nardiello, Giampaolo Piotto, Luigi R. Bedin, Edo Berger, and Rishi Paudel. 2016. Wisep j060738.65+242953.4: A Nearby Pole-on L8 Brown Dwarf With Radio Emission. The Astronomical Journal 152, no. 5: 123. doi:10.3847/0004-6256/152/5/123.
Published Version	doi:10.3847/0004-6256/152/5/123
Citable link	http://nrs.harvard.edu/urn-3:HUL.InstRepos:30510301
Terms of Use	This article was downloaded from Harvard University's DASH repository, and is made available under the terms and conditions applicable to Open Access Policy Articles, as set forth at http://nrs.harvard.edu/urn-3:HUL.InstRepos:dash.current.terms-of-use#OAP

arXiv:1607.00943v1 [astro-ph.SR] 4 Jul 2016

WISEP J060738.65+242953.4: A NEARBY, POLE-ON L8 BROWN DWARF WITH RADIO EMISSION

John E. Gizis
Department of Physics and Astronomy, University of Delaware, Newark, DE 19716, USA

Peter K. G. Williams
Harvard-Smithsonian Center for Astrophysics, 60 Garden Street, Cambridge, MA 02138, USA

Adam J. Burgasser
Center for Astrophysics and Space Science, University of California San Diego, La Jolla, CA 92093, USA

Mattia Libralato[1], Domenico Nardiello[1], Giampaolo Piotto[1]
Dipartimento di Fisica e Astronomia, Università di Padova, Vicolo dell'Osservatorio 3, Padova, I-35122, Italy

Luigi R. Bedin
INAF-Osservatorio Astronomico di Padova, Vicolo dell'Osservatorio 5, Padova, I-35122, Italy

Edo Berger
Harvard-Smithsonian Center for Astrophysics, 60 Garden Street, Cambridge, MA 02138, USA

Rishi Paudel
Department of Physics and Astronomy, University of Delaware, Newark, DE 19716, USA
Accepted to AJ

ABSTRACT

We present a simultaneous, multi-wavelength campaign targeting the nearby (7.2 pc) L8/L9 (optical/near-infrared) dwarf WISEP J060738.65+242953.4 in the mid-infrared, radio, and optical. Spitzer Space Telescope observations show no variability at the 0.2% level over 10 hours each in the 3.6 and 4.5 micron bands. *Kepler* K2 monitoring over 36 days in Campaign 0 rules out stable periodic signals in the optical with amplitudes great than 1.5% and periods between 1.5 hours and 2 days. Non-simultaneous Gemini optical spectroscopy detects lithium, constraining this L dwarf to be less than ~ 2 Gyr old, but no Balmer emission is observed. The low measured projected rotation velocity ($v \sin i < 6$ km s^{-1}) and lack of variability are very unusual compared to other brown dwarfs, and we argue that this substellar object is likely viewed pole-on. We detect quiescent (non-bursting) radio emission with the VLA. Amongst radio detected L and T dwarfs, it has the lowest observed L_ν and the lowest $v \sin i$. We discuss the implications of a pole-on detection for various proposed radio emission scenarios.

Subject headings: brown dwarfs — starspots — stars: activity — stars: individual: WISEP J060738.65+242953.4 — solar neighborhood

1. INTRODUCTION

Brown dwarfs are doomed to steadily cool and fade by their lack of hydrogen fusion, but they nevertheless exhibit a wide variety of non-equilibrium, time-dependent behaviors. Their mineral and metal condensate clouds are not completely uniform, resulting in periodic variability and "weather" (Buenzli et al. 2014; Metchev et al. 2015). The dramatic differences in observed spectra at the L/T transition are typically attributed to changes in the qualitative properties of clouds (Tsuji et al. 1999; Burrows et al. 2000; Allard et al. 2001; Ackerman & Marley 2001; Burgasser et al. 2002; Knapp et al. 2004). In some cases, rapid, high-amplitude variability is observed (Radigan et al. 2014). These cloud changes are so signifi-

cant that they may even affect the luminosity evolution of the brown dwarf itself (Saumon & Marley 2008; Dupuy et al. 2015). Meanwhile, magnetic fields are generated even in L and T dwarfs, resulting in surprisingly strong, variable radio emission (Berger 2002; McLean et al. 2012; Williams & Berger 2015; Kao et al. 2016).

Deeper understanding of these phenomena requires both surveys of typical ultracool (later than M7) dwarfs and detailed studies of particularly favorable targets. One such target is the nearby brown dwarf WISEP J060738.65+242953.4 (Castro & Gizis 2012, hereafter W0607+24). Classified as L8 in the optical and L9 in the near-infrared, with a preliminary trigonometric parallax placing it at a distance of $7.19^{+0.11}_{-0.10}$ pc (Castro et al. 2013), W0607+24 is the nearest known late-L dwarf northern hemisphere, and the third-nearest on the whole

[1] INAF-Osservatorio Astronomico di Padova, Vicolo dell'Osservatorio 5, Padova, I-35122, Italy

sky. W0607+24 is therefore a prime target in understanding the physics of the L/T transition, across which mineral condensate clouds are believed to sink below the photosphere (see Tremblin et al. 2016 for an alternate, cloudless model). W0607+24 also lies close to the ecliptic plane, in the K2 mission (Howell et al. 2014) Campaign 0 field. Although designed to search for transiting planets around bright Sun-like stars, the *Kepler* space telescope (Koch et al. 2010) can also obtain long time-series photometry of fainter targets that happen to lie in the field of view. Indeed, during its original mission, it was able to measure rotational modulations due to photospheric spots in late-M (Martín et al. 2013) and L1 (Gizis et al. 2013) very-low-mass stars. Each K2 field offers the opportunity to monitor additional very-low-mass stars or brown dwarfs. K2 Campaign 2 monitoring of Upper Scorpius has detected variability in 16 young, M-type brown dwarfs (Scholz et al. 2015). Motivated by the K2 observations of W0607+24, we observed it simultaneously with the Karl G. Jansky Very Large Array (VLA)[2] and the Spitzer Space Telescope (Werner et al. 2004). In this paper, we present the results of ground-based spectroscopy and the simultaneous multi-wavelength observations.

2. DATA AND OBSERVATIONS

2.1. *Spectroscopy*

We observed W0607+24 on UT Date 2012 October 15 with the Gemini-North telescope (Gemini program GN-2012B-Q-105) and the GMOS spectrograph (Hook et al. 2004) using grating R831. The wavelength coverage was 6340 to 8460Å with a resolution of ~ 2Å. We processed it using standard IRAF Gemini tasks and co-added the four 600 second exposures. Conditions were non-photometric. The spectrum (Figure 1) is consistent with the L8 optical spectral type previously reported (Castro et al. 2013). We detect lithium absorption (equivalent width EW 4.0± 0.4 Å, Table 1). There is no detectable Hα emission or absorption (EW < 0.5Å).

We observed W0607+24 on UT date 2013 October 16 with the Keck II NIRSPEC near-infrared echelle spectrograph (McLean et al. 2000) in partly cloudy conditions and excellent seeing (0″.5) at 2 μm. The high-dispersion mode was used with the 0″.432×12″ slit and N7 filter to obtain 2.00–2.39 μm spectra over orders 32–38 with $\lambda/\Delta\lambda = 20,000$ ($\Delta v = 15$ km s^{-1}) and dispersion of 0.315 Å pixel^{-1}. Two 900 s exposures were obtained at an airmass of 1.03 in two nods separated by 7″ along the slit, and the nearby A0 V star HD 43584 ($V = 5.11$) was observed for telluric and flux calibration. Raw data frames were reduced and combined following standard procedures, and spectra in order 33 (2.293–2.320 μm) were optimally extracted. The 1D uncalibrated spectrum was then fit to a suite of spectral templates constructed from the BT-Settl atmosphere models (Allard et al. 2011; Allard 2014), telluric absorption modeled from the Solar atlas of Livingston & Wallace (1991), and a 2nd-order polynomial continuum, using a Markov-Chain Monte Carlo (MCMC) code

with Metropolis-Hastings algorithm; see Burgasser et al. (2015b) for details. We compared solar-metallicity models in the $T_{\rm eff} = 1300$–2100 K and $\log g = 4.0$–5.5 (cgs) ranges. Both wavelength scale, source $v_{\rm rad}$ and $v \sin i$ rotational broadening were allowed to vary to minimize χ^2 residuals. The spectrum in the MCMC simulation with the lowest residuals is shown in Figure 2 to illustrate the quality of the fits. The outcome of the MCMC simulation is the posterior probability density function for the five-dimensional parameter space. By marginalizing (integrating) over the other parameters, we find mean values of $v_{\rm rad} = -11.9\pm1.1$ km s^{-1} and $v \sin i = 6\pm2$ km s^{-1}. However, the last value is suspect, as the broadening profile is actually smaller than the instrumental profile. W0607+24 has the narrowest lines observed so far in the ongoing survey of Burgasser et al. (2012), so we conservatively claim a limit on the rotational broadening of $v \sin i < 6$ km s^{-1}.

2.2. *Radio Observations and Analysis*

We observed W0607+24 with the VLA for 1.5 hr starting at UT date 2014 May 23 22:04 (BMJD 56800.9298; program 14A-541) using two frequency windows of 1 GHz bandwidth each, centered at 5.0 and 7.1 GHz. The gain and phase calibrator was J0559+2353 and the bandpass and flux density calibrator was 3C 138. We calibrated the data using standard techniques in the CASA software environment (McMullin et al. 2007), using the "Perley-Butler 2010" flux density scale (Perley & Butler 2013) and flagging RFI automatically using the **aoflagger** tool (Offringa et al. 2010, 2012). After imaging the calibrated visibilities, we detect a 3.5σ source $0.6''$ distant from the predicted position of W0607+24 having a total flux density of 15.6 ± 6.3 μJy at a mean frequency of 6.05 GHz, where the flux density uncertainty is determined from non-linear least squares modeling of the image data. Imaging the two spectral windows separately, we measure flux densities of 16.5 ± 7.6 and 15.6 ± 10.7 μJy at 5.0 and 7.1 GHz, respectively, corresponding to a limit on the spectral index $|\alpha| \lesssim 2$. We imaged the Stokes V data, finding no evidence for circularly polarized emission from W0607+24 in an image with rms noise of 4.5 μJy, leading to a 3σ limit on the fractional circular polarization of $|V|/I \lesssim 90\%$. We extracted a radio light curve for W0607+24 using the technique described in Williams et al. (2013) and found no evidence of variability.

2.3. *Mid-Infrared Photometry*

We observed W0607+24 with the IRAC camera (Fazio et al. 2004) under Spitzer DDT program 10167 for twenty hours on UT Dates 2014 May 23-24. The principal limit to high precision relative photometry with IRAC is intra-pixel sensitivity variations coupled to telescope pointing changes (Grillmair et al. 2012; Ingalls et al. 2012). We designed the observations using the procedures developed by the Spitzer Science Center (SSC). W0607+24 was placed on the IRAC "sweet spot" (pixels $X = 23$, $Y = 231$). Following a thirty minute staring observation to allow the telescope to settle, we observed with IRAC Channel 1 (hereafter [3.6]) for 2709 twelve-second exposures starting at BMJD 56800.8010689 (after discarding the first frame). We then re-positioned the telescope and observed with IRAC channel 2 (hereafter [4.5]) for 1082 thirty-second exposures starting at
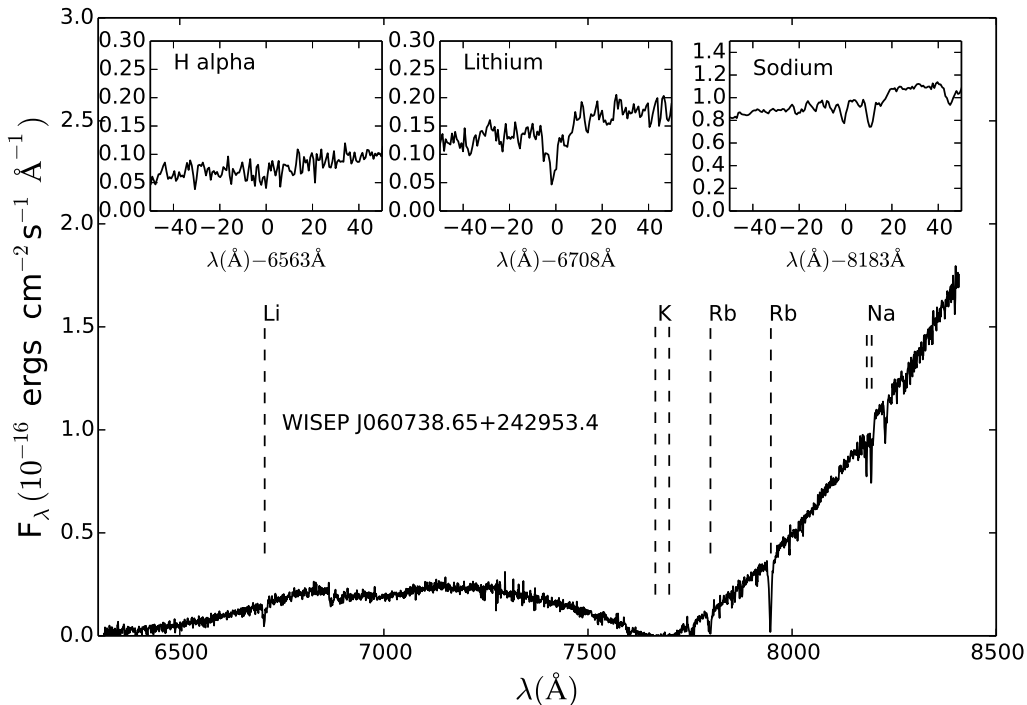
Figure 1. Optical spectrum of W0607+24. We detect lithium absorption but no Hα emission or absorption.

BMJD 56801.2149001. We measured the target centroid using the box centroider software provided by SSC and then measured aperture photometry with a radius of 3 pixels. We analyzed the photometry following the techniques described by Heinze et al. (2013). First, outliers are rejected by a robust fitting algorithm. We then median smoothed the centroids on a four-to-five minute timescale (combining 25 observations for [3.6] and 7 for [4.5]), a period much shorter than the instrumental or astrophysical timescales. We find that the telescope pointing has a 53 minute periodic component with an amplitude of 0.02 pixels in X and Y; additionally, over ten hours there is a drift of 0.05 pixels in X and 0.06 pixels in Y. We then modeled the pixel phase photometric shift in each band with a linear function in X and Y, which removed the correlation of the measured photometry with the telescope pointing. In Figure 3, we plot the measured relative photometry, where we have normalized each band by its median value. The histogram shows the data averaged over 30 measurements for [3.6] and 12 points for [4.5]. (The individual [3.6] points are noisier due to the shorter exposure time.) We find that the brightness of W0607+24 is constant in time for both bands (Figure 3). The standard deviation of the averaged [3.6] data is 0.12% and the [4.5] data is 0.13%.

To convert our 3-pixel aperture photometry to calibrated Vega-system magnitudes on the Reach et al. (2005) system, we use the SSC aperture corrections and the SSC array location-dependent photometric correction to find that W0607+24 has $m_{[3.6]} = 11.13$ and $m_{[4.5]} = 10.95$. The uncertainties in these magnitudes are dominated by systematic uncertainties in the corrections, $\sim \pm 0.03$ mag. The observed color of 0.18 is similar to other L8 dwarfs measured by Patten et al. (2006).

We do not observe any significant evidence of variability, whether due to rotation or "weather." To quantify the variability limits, we use a Markov Chain Monte Carlo simulation to generate sine function fits to each of the bands. Each sine curve has the form $a_0 + a_1 \sin(t/P + \phi))$ with periods $0 < P < 1$ days for Spitzer. After an initial burn-in of 2000 steps, we run one million steps. For Spitzer [3.6], 99% of the fits have amplitude $a_1 < 0.0019$. Similarly, for Spitzer [4.5], 99% of the fits have $a_1 < 0.0017$. This rules out rotational variability at the levels ($> 0.2\%$) seen in most L dwarfs (Metchev et al. 2015).

2.4. *Optical Photometry*

W0607+24 was monitored in K2 Campaign 0 as source 202059521 under program GO0008. For each 30-minute long cadence exposure (Jenkins et al. 2010), a 22 by 21 pixel aperture was saved. Each pixel is 4 by 4 arcseconds. Folding the observed W0607+24 optical spectrum from Castro et al. (2013) through the *Kepler* spectral response curve (Koch et al. 2010) and scaling from the observed *Kepler* count rate (550 DN s^{-1}) for the L1 dwarf WISEP J190648.47+401106.8 (Gizis et al. 2013, W1906+40), we expect a K2 count rate of ~ 100 DN s^{-1}. As shown in Figure 4, it is the red tail of the Kepler filter that allows a detection; we calculate that the effective wavelength of the Kepler filter is 832 nm for W0607+24. However, crowding is important at W0607+24's low galactic latitude (Figure 5). The brightest star in the Kepler image, SDSS J060738.06+242939.5 ($r = 13.66$), is only 16 arcseconds away. In addition there are three fainter stars between 6 and 8 arc seconds away from W0607+24: SDSS J060738.72+242947.2 ($r = 18.67$), SDSS J060738.18+242957.5 ($r = 19.83$),
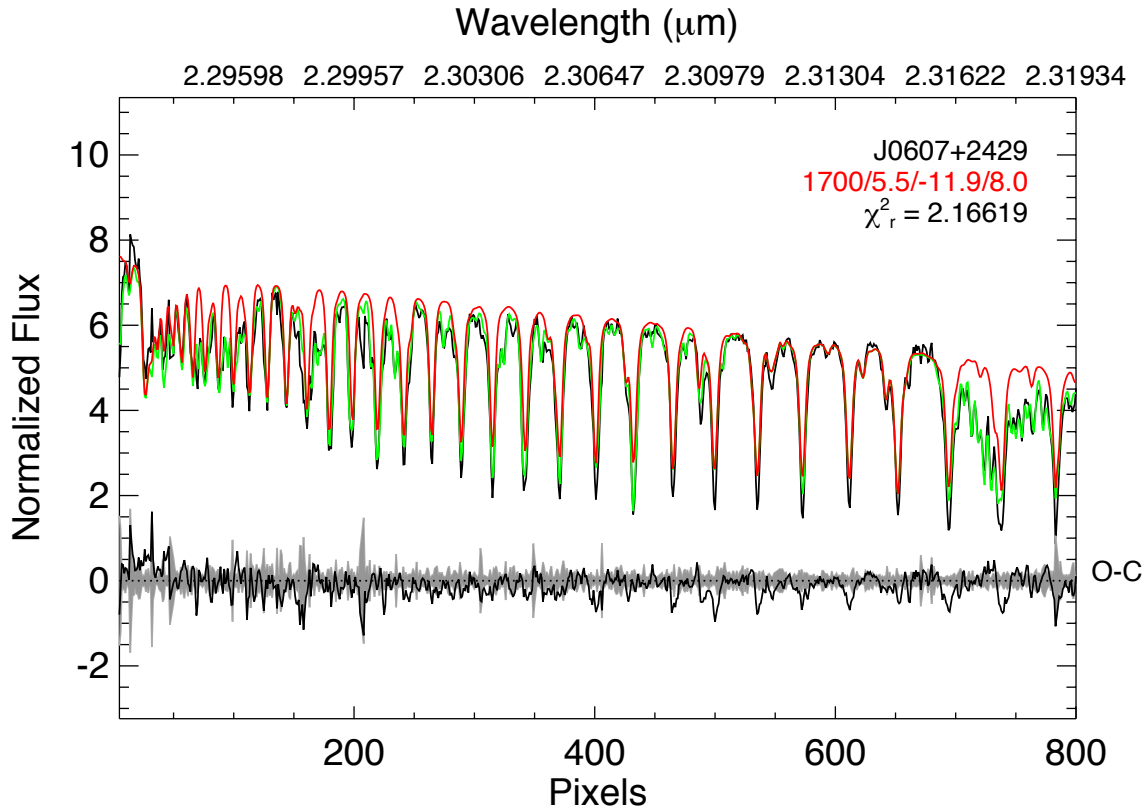
Figure 2. NIRSPEC spectrum of W0607+24 (black line) with a model without (red) and with (green) telluric absorption. Pixel scale is listed along the bottom while wavelength scale is listed along the top. The difference between data and model (O-C) is shown in black at the bottom of the plot; the $\pm 1\sigma$ uncertainty spectrum is shown in grey.

Table 1
WISEP J060738.65+242953.4

Parameter	W0607+24	Remarks
Sp. Type (nIR)	L9	Castro et al. (2013)
Sp. Type (opt)	L8	Castro et al. (2013)
π_{abs}	138 ± 2	mas, Castro et al. (2013)
$v_{\rm rad}$	-11.9 ± 1.1	km s^{-1}
$v \sin i$	< 6	km s^{-1}
EW Lithium	4.0 ± 0.4	Å
EW Hα	< 0.5	Å
$\log L_\nu$	12.0 ± 0.2	erg s^{-1} Hz^{-1}
$\log L_\nu/L_{\rm bol}$	-16.9 ± 0.2	Hz^{-1}
U	$+12.9 \pm 1.3$	km s^{-1}
V	-0.7 ± 0.6	km s^{-1}
W	-20.0 ± 0.5	km s^{-1}
K_P	19.73 ± 0.08	mag
$m_{[3.6]}$	11.13 ± 0.03	mag
$m_{[4.5]}$	10.95 ± 0.03	mag
m_{bol}	15.70 ± 0.03	mag
$\log L/L_\odot$	-4.66 ± 0.02	
$\log L_{\rm H\alpha}/L_{\rm bol}$	$< 3 \times 10^{-7}$	
Age	< 2	Gyr
Mass	≤ 0.055	$M_\odot$

and SDSS J060738.09+242953.8 ($r = 18.26$).

Libralato et al. (2016) have demonstrated that effective pixel-convolved PSF (ePSF, Anderson & King 2000) neighbor-subtraction with a high angular resolution input star list allows photometry of even faint stars in the K2 Campaign 0 observations of open cluster M 35 and NGC 2158. W0607+24 is on the same K2 detector as M 35, so we use the same ePSF models and methodology. The input star catalog comes from the high-angular-resolution input star list from the Asiago Schmidt telescope used in the M 35 analysis (*Asiago Input Catalog*, Nardiello et al. 2015), but W0607+24's position is updated with an early 2015 image. After subtracting the neighbor stars, we measured both ePSF-fit and aperture (1 pixel) photometry for W0607+24; these are consistent, so we base the remainder of our analysis on the ePSF photometry results. We use only the data from the final 36 days of Campaign 0 (*Kepler* mission times 1935.9 to 1972.2) during which the highest-quality data were collected. We discard all photometry during thruster fires and de-trend the drift-induced effects as in Libralato et al. (2016) using the data for all stars in the M35 region; this removes the spurious instrumental periodic 5.9-hour
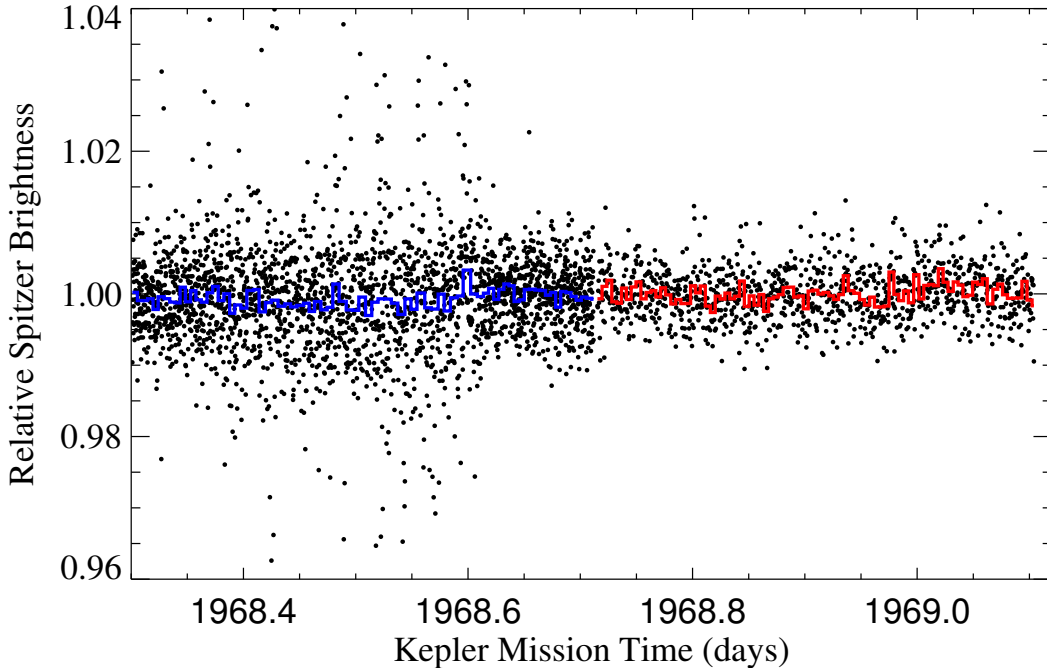
Figure 3. Spitzer photometry of W0607+24. The individual frame measurements are shown as points and the averaged photometry (blue for [3.6], red for [4.5]) is shown as a histogram. There is no evidence of variability in this brown dwarf in either band. The time series begins at BMJD 56800.8010689.

signal. (See Vanderburg & Johnson (2014) for a discussion of the effects of drift on the photometry.) Applying the Libralato et al. (2016) instrumental calibration the median observed K2 magnitude of W0607+24 is $K_P = 19.72$. Similar magnitude M35 stars have point-to-point root-mean-square of $\sim 3\%$. The K2 photometry during the time period of the Spitzer observations is shown in Figure 6. It is consistent with a constant light curve and the expected noise. Over the full 36 day period, the photometry drifts by 0.12 magnitude, mainly before day 1955. This drift is correlated with the systematic change of the positions of the stars on the detectors and we therefore attribute it to the instrumental effects. The *Kepler* median count rates of Gizis et al. (2015) for W1906+40 varied by ±0.08 mags for different spacecraft quarters, so we adopt this as the uncertainty for the W0607+24 photometry. Searching both the entire dataset, ten day subsets, and five day subsets, there are no significant periodogram peaks for periods < 2 days in the K2 data. The light curve after day 1955 is shown in Figure 7. We show a non-parametric Nadaraya-Watson kernel regression (computed using the PyQt package; see Feigelson & Babu 2012 for a discussion of this statistical method); the $\sim 2\%$ variations on week-long timescales can be attributed to the K2 pointing drift. Simulations similar to those of Section 2.3 show stable sinusoidal signals with periods less than 2 days and amplitudes > 1.4% can be ruled out.

3. DISCUSSION

3.1. *The orientation of W0607+24*

The spectroscopy of W0607+24 indicates it is a typical L8-L9 dwarf. Integrating the observed spectra and photometry, we find that the luminosity is $\log L_{\rm bol}/L_\odot =$
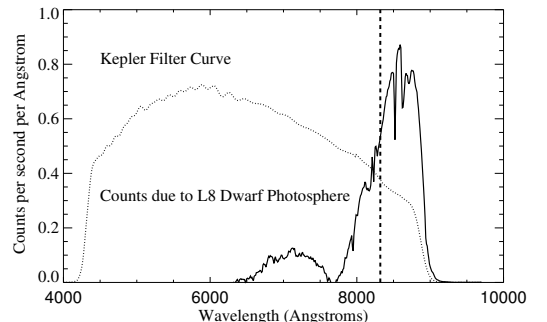

Figure 4. The predicted counts as a function of wavelength for W0607+24 (solid curve). The optical spectrum of Castro et al. (2013) has been folded through the *Kepler* filter curve (dotted). The effective wavelength of 8320Å for this target is shown as a dashed line.

-4.66 ± 0.02. This luminosity and the detection of lithium together imply it is at or below the lithium-burning limit ($M \leq 0.055 M_\odot$) with an age less than 2 billion years according to evolutionary models (Burrows et al. 1997; Baraffe et al. 2003; Saumon & Marley 2008). These models also predict the radius, $R \approx 0.1 R_\odot$.

The observed projected rotation period and the model radius imply a rotation period of $P > 20$ hours if $i = 90°$, or $P > 16$ hours for the expected stellar average $\sin i = \pi/4$. Although we cannot directly rule out such a slow rotation, it is in conflict with our prior expectations from other studies of brown dwarfs. Very few brown dwarfs have low $v \sin i$: Reiners & Basri (2008) found 1 of 45 L dwarfs have $v \sin i < 3$ km s^{-1}; Blake et al. (2010) found 4 of 57 L dwarfs have $v \sin i < 9$ km s^{-1}; Zapatero Osorio et al. (2006) had 1 of 15 L and T dwarfs with
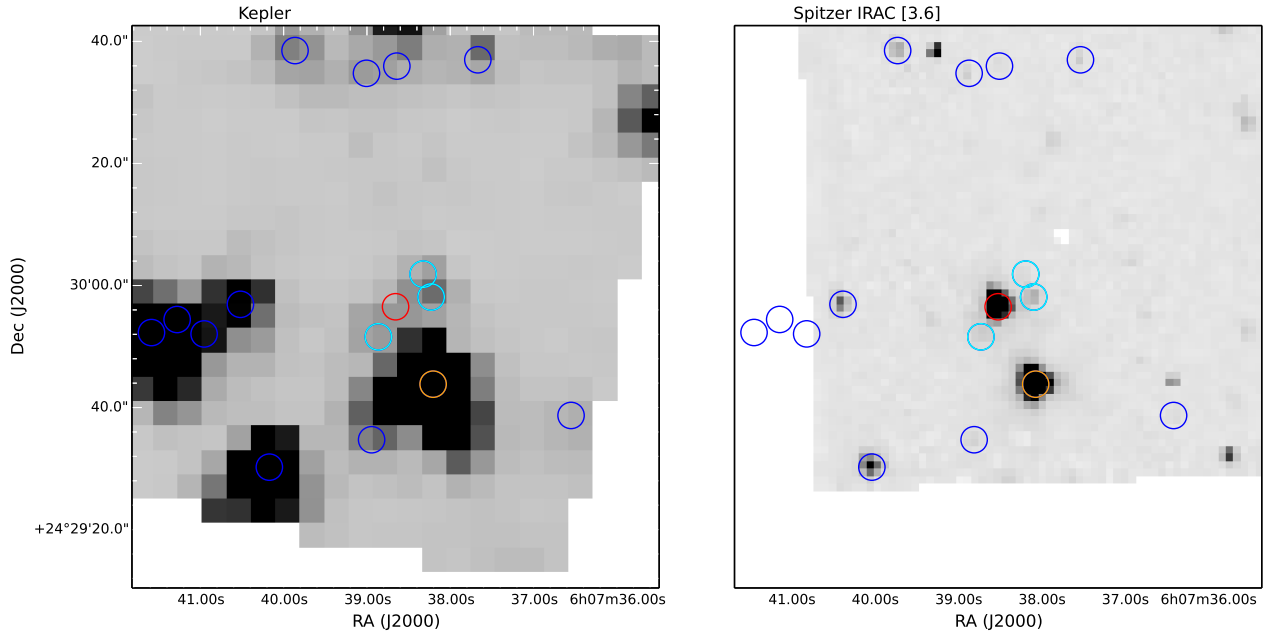
Figure 5. K2 and Spitzer [3.6] images of W0607+24. The position of W0607+24 is marked by a red circle. SDSS J060738.06+242939.5, marked by an orange circle, is the brightest star in the K2 image. The three faint ($r = 18.3 - 19.6$) stars marked by cyan circles, contribute significant flux to the K2 measurement but are negligible at Spitzer's longer wavelength and higher resolution. Other stars with $r < 20$ in SDSS are marked with blue circles.
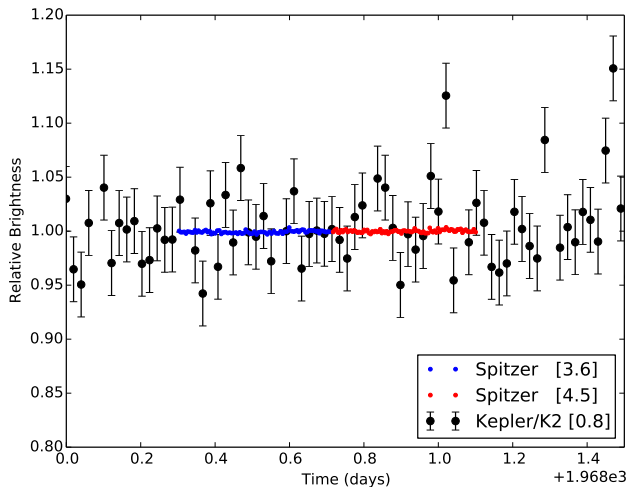

Figure 6. *K2* photometry compared with Spitzer photometry. The *K2* data are consistent with a constant light curve with an uncertainty (standard deviation) of 3.7%.
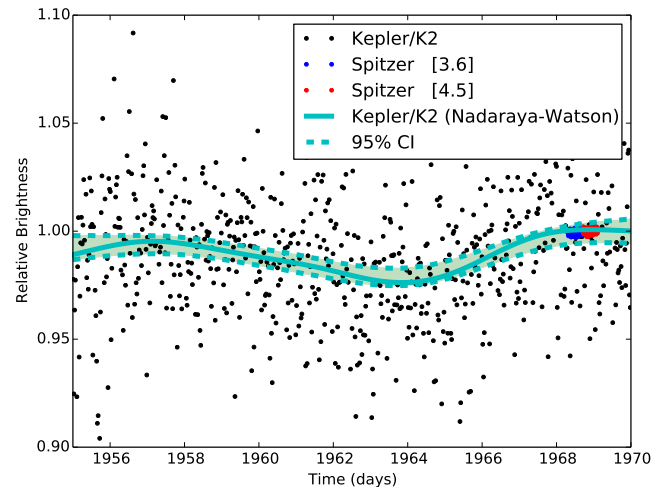
Figure 7. K2 photometry of W0607+24 for a 15 day period with the most stable spacecraft pointing. The non-parametric Nadaraya-Watson kernel regression of the trend is shown. We find no evidence of a long rotation period ($P > 10$ hr). The long-term variations are most likely to due to systematic instrumental (pointing) effects.

$v \sin i < 15$ km s^{-1}. Radigan et al. (2014) argue that these collective $v \sin i$ measurements are consistent with a single log-normal distribution peaked at $P = 4.1$ hrs with $\sigma_{\ln P} = 0.48$. If we simulate ten million randomly inclined objects[3] with radius $R = 0.1 R_\odot$ drawn from this log-normal period distribution, we find that 3.4% have $v \sin i < 6$ km s^{-1}. The distribution of true periods and inclinations for the simulated objects with $v \sin i < 6$ km s^{-1} is given in Table 2. This distribution corresponds

to the Bayesian posterior probabilities given the prior period distribution and the evidence of the observed $v \sin i$. There is only a 5% chance of a period of 15 hours or greater; on the other hand, there is a 77% chance that $i < 20°$. The median rotation period for these objects is 6.6 hours; the average is 7.5 hours. We therefore argue that most likely we are viewing W0607+24 close to pole-on. This also explains the lack of variability in the two Spitzer bands, which is otherwise surprising. Based on their Spitzer 3-5μm monitoring of a large sample of L

[3] If x is a randomly generated real number between 0 and 1 with a uniform distribution, then $\cos i = 2x - 1$.

and T dwarfs, Metchev et al. (2015) conclude that spots are present on "virtually 100% of L3 – L9.5 dwarfs" and that their non-detections can be explained by viewing geometry. This would suggest that the probabilities of long periods and $i > 20°$ in Table 2 are overestimated and favors the pole-on scenario.

3.2. *Implications of Radio Emission*

The flux density of our radio detection of W0607+24 corresponds to a spectral luminosity of $10^{12.0\pm0.2}$ erg s^{-1} Hz^{-1} and $L_\nu/L_{\rm bol} = 10^{-16.9\pm0.2}$ Hz^{-1}. Figure 8 places this result in context by comparing W0607+24 to other ultracool dwarfs with measurements of both radio emission and rotation. It is an unusual object in several respects: of the radio-detected L and T dwarfs it has the lowest L_ν, it is the only radio-detected ultracool dwarf for which a measurement of $v \sin i$ has yielded an upper limit rather than a detection, and it is the only radio-detected ultracool dwarf without an Hα detection ($\log L_{\rm H\alpha}/L_{\rm bol} < 3 \times 10^{-7}$). Only the M9.5 dwarf WISE J072003.20−084651.2 has been detected at a lower radio spectral luminosity (Burgasser et al. 2015a). While W0607+24 is clearly one of the most radio-faint ultracool dwarfs yet detected — an unsurprising fact given its proximity — two effects combine to cause it to appear relatively radio-bright in the lower-right ($L_\nu/L_{\rm bol}$ vs. $v \sin i$) panel of Figure 8: its has unusually low values of both $L_{\rm bol}$ and $v \sin i$. The low $v \sin i$ of W0607+24 is particularly worthy of note because, as we have described, it may in fact be due to a nearly pole-on viewing geometry rather than slow rotation.

W0607+24 is a valuable test case for understanding the mechanisms of radio emission in ultracool dwarfs. Some of the radio-detected objects emit rapid, intense bursts with high circular polarization, often found to occur periodically (Hallinan et al. 2006, 2008; Berger et al. 2009; Williams & Berger 2015) and attributed to coherent emission due to the electron cyclotron maser instability (ECMI; Wu & Lee 1979; Treumann 2006). Assuming that ECMI bursts propagate perpendicular to the magnetic field and originate near closely-aligned rotational and magnetic poles, they may only be detectable from ultracool dwarfs with $i \approx 90°$. There is evidence for high inclinations in three of the well-known ECMI-bursting sources (TVLM 513–46546, 2MASS J00361617+1821104, and LSR J1835+3259; Hallinan et al. 2008). If the orientation of W0607+24 is truly pole-on, the detection of an ECMI burst from it would be surprising in this context.

Ultracool dwarfs can also produce steady, broadband emission with weak to moderate polarization, as we have detected here. This emission is generally interpreted as being due to the gyrosynchrotron mechanism (e.g., Berger 2002; Osten et al. 2006; Burgasser et al. 2013); assuming a pole-on orientation, our detection casts further doubt on the alternative hypothesis that the emission is actually depolarized, steady ECMI emission (Hallinan et al. 2006, 2008). Regardless of the mechanism, there is little insight as to the geometry of the non-flaring emission region in these objects: its area is likely a few times that of the (sub)stellar disk (e.g., Berger 2002), and rotational modulation suggests that it is not totally axisymmetric (e.g., McLean et al. 2011). The relative radio-faintness of W0607+24 may be due to its orienta-

tion if the emission is concentrated at the poles as has been inferred for Algol from VLBI data (Mutel et al. 1998).

Meanwhile, if W0607+24 is instead truly a slow rotator rather than orienated pole-on ($P \gtrsim 32$ hours as per Section 3.1), it would be the slowest-rotating ultracool dwarf with a radio detection, with a rotation period $\gtrsim 8$ times longer than that of NLTT 33370 B (Williams et al. 2015), although several radio-active dwarfs have no rotation measurements available. Assuming a convective turnover timescale $\tau_c = 70$ days, its Rossby number Ro $= P/\tau_c \gtrsim 0.02$, high but not unheard-of within the radio-active ultracool sample (Cook et al. 2014) and still well within the rotation-independent regime inferred from some geodynamo simulations (Christensen & Aubert 2006). Its radio luminosity is just consistent with the slowly-rotating and X-ray flaring "group B" categorization of Stelzer et al. (2012), although the possibility of detecting X-rays from this object seems remote given the dramatic drop in L_X with temperature (Berger et al. 2010; Williams et al. 2014).

4. CONCLUSIONS

Although a typical late-L dwarf in most respects, W0607+24's unusually sharp lines and lack of variability is consistent with a viewing angle near pole-on. As the nearest known northern hemisphere late-L dwarf, this offers many possibilities for future studies. For example, it could serve as an useful standard for line-broadening and polarization studies. If there is a planetary system aligned with the primary's rotation axis, then we would expect very little radial velocity signal but a strong astrometric signal. Further follow-up is needed to confirm and better characterize the radio emission.

The *Kepler* and K2 studies of the L dwarfs W1906+40 and W0607+24 demonstrate the value of space-based monitoring with long time baselines. We are monitoring additional late-M and L dwarfs in other K2 campaigns. They are more distant than W0607+24, but because they are warmer, some are brighter and higher signal-to-noise than W0607+24. In addition, most K2 fields are less crowded than Campaign 0. The most promising potential brown dwarf target for K2 is the nearby L5 dwarf 2MASSW J1507476-162738 (Reid et al. 2000), one of the brightest and best-studied L dwarfs. It is known to be rapid rotator ($P = 2.5$ hr) seen to be spotted in some epochs (Metchev et al. 2015) but not others (Koen 2013). It could be observed in K2 Campaign 15, where we would expect to detect clear signatures of rotational modulation and spot evolution over the three month campaign.

Table 2
Period/Inclination Posterior Probabilties

Period (hr)	Any i	$i < 5°$	$5° \leq i < 10°$	$10° \leq i < 20°$	$i \geq 20°$
Any P	100%	11%	26%	40%	22%
$P < 5$	28%	7%	15%	6%	0%
$5 \leq P < 7.5$	32%	3%	8%	21%	0%
$7.5 \leq P < 10$	20%	1%	2%	10%	7%
$10 \leq P < 15$	15%	0.3%	1%	4%	10%
$P \geq 15$	5%	0%	0.1%	0.4%	5%

in part on observations obtained at the Gemini Observatory, which is operated by the Association of Universities for Research in Astronomy (AURA) under a cooperative agreement with the NSF on behalf of the Gemini partnership: the National Science Foundation (United States), the Science and Technology Facilities Council (United Kingdom), the National Research Council (Canada), CONICYT (Chile), the Australian Research Council (Australia), CNPq (Brazil) and CONICET (Argentina). Some of the data presented herein were obtained at the W.M. Keck Observatory, which is operated as a scientific partnership among the California Institute of Technology, the University of California and the National Aeronautics and Space Administration. The Observatory was made possible by the generous financial support of the W.M. Keck Foundation. The National Radio Astronomy Observatory is a facility of the National Science Foundation operated under cooperative agreement by Associated Universities, Inc.

This research has made use of NASA's Astrophysics Data System, the VizieR catalogue access tool, CDS, Strasbourg, France, IRAF, PyQt, and Astropy, a community-developed core Python package for Astronomy (Astropy Collaboration et al. 2013). IRAF is distributed by the National Optical Astronomy Observatory, which is operated by the Association of Universities for Research in Astronomy (AURA) under cooperative agreement with the National Science Foundation. IRAF is distributed by the National Optical Astronomy Observatory, which is operated by the Association of Universities for Research in Astronomy (AURA) under cooperative agreement with the National Science Foundation. This work made use of PyKE (Still & Barclay 2012), a software package for the reduction and analysis of Kepler data. This open source software project is developed and distributed by the NASA Kepler Guest Observer Office. This research made use of Montage, funded by the National Aeronautics and Space Administration's Earth Science Technology Office, Computation Technologies Project, under Cooperative Agreement Number NCC5-626 between NASA and the California Institute of Technology. Montage is maintained by the NASA/IPAC Infrared Science Archive. This research made use of APLpy, an open-source plotting package for Python hosted at http://aplpy.github.com

Facilities: EVLA, Gemini:Gillett (GMOS), Keck:II (NIRSPEC), Kepler, Spitzer (IRAC)

REFERENCES

Ackerman, A. S., & Marley, M. S. 2001, ApJ, 556, 872
Allard, F. 2014, in IAU Symposium, Vol. 299, IAU Symposium, ed. M. Booth, B. C. Matthews, & J. R. Graham, 271
Allard, F., Hauschildt, P. H., Alexander, D. R., Tamanai, A., & Schweitzer, A. 2001, ApJ, 556, 357
Allard, F., Homeier, D., & Freytag, B. 2011, in Astronomical Society of the Pacific Conference Series, Vol. 448, 16th Cambridge Workshop on Cool Stars, Stellar Systems, and the Sun, ed. C. Johns-Krull, M. K. Browning, & A. A. West, 91
Anderson, J., & King, I. R. 2000, PASP, 112, 1360
Astropy Collaboration, Robitaille, T. P., Tollerud, E. J., et al. 2013, A&A, 558, A33
Baraffe, I., Chabrier, G., Barman, T. S., Allard, F., & Hauschildt, P. H. 2003, A&A, 402, 701
Berger, E. 2002, ApJ, 572, 503
Berger, E., Rutledge, R. E., Phan-Bao, N., et al. 2009, ApJ, 695, 310
Berger, E., Basri, G., Fleming, T. A., et al. 2010, ApJ, 709, 332
Blake, C. H., Charbonneau, D., & White, R. J. 2010, ApJ, 723, 684
Buenzli, E., Apai, D., Radigan, J., Reid, I. N., & Flateau, D. 2014, ApJ, 782, 77
Burgasser, A. J., Luk, C., Dhital, S., et al. 2012, ApJ, 757, 110
Burgasser, A. J., Marley, M. S., Ackerman, A. S., et al. 2002, ApJ, 571, L151
Burgasser, A. J., Melis, C., Todd, J., et al. 2015a, AJ, 150, 180
Burgasser, A. J., Melis, C., Zauderer, B. A., & Berger, E. 2013, ApJ, 762, L3
Burgasser, A. J., Gillon, M., Melis, C., et al. 2015b, AJ, 149, 104
Burrows, A., Marley, M. S., & Sharp, C. M. 2000, ApJ, 531, 438
Burrows, A., Marley, M., Hubbard, W. B., et al. 1997, ApJ, 491, 856
Castro, P. J., & Gizis, J. E. 2012, ApJ, 746, 3
Castro, P. J., Gizis, J. E., Harris, H. C., et al. 2013, ApJ, 776, 126
Christensen, U. R., & Aubert, J. 2006, Geophysical Journal International, 166, 97
Cook, B. A., Williams, P. K. G., & Berger, E. 2014, ApJ, 785, 10
Dupuy, T. J., Liu, M. C., Leggett, S. K., et al. 2015, ApJ, 805, 56
Fazio, G. G., Hora, J. L., Allen, L. E., et al. 2004, ApJS, 154, 10
Feigelson, E. D., & Babu, G. J. 2012, Modern Statistical Methods for Astronomy (Cambridge University Press)
Gizis, J. E., Burgasser, A. J., Berger, E., et al. 2013, ApJ, 779, 172
Gizis, J. E., Dettman, K. G., Burgasser, A. J., et al. 2015, ApJ, 813, 104
Grillmair, C. J., Carey, S. J., Stauffer, J. R., et al. 2012, in Society of Photo-Optical Instrumentation Engineers (SPIE) Conference Series, Vol. 8448, Society of Photo-Optical Instrumentation Engineers (SPIE) Conference Series
Hallinan, G., Antonova, A., Doyle, J. G., et al. 2006, ApJ, 653, 690
—. 2008, ApJ, 684, 644
Heinze, A. N., Metchev, S., Apai, D., et al. 2013, ApJ, 767, 173
Hook, I. M., Jørgensen, I., Allington-Smith, J. R., et al. 2004, PASP, 116, 425
Howell, S. B., Sobeck, C., Haas, M., et al. 2014, PASP, 126, 398
Ingalls, J. G., Krick, J. E., Carey, S. J., et al. 2012, in Society of Photo-Optical Instrumentation Engineers (SPIE) Conference Series, Vol. 8442, Society of Photo-Optical Instrumentation Engineers (SPIE) Conference Series
Jenkins, J. M., Caldwell, D. A., Chandrasekaran, H., et al. 2010, ApJ, 713, L120
Kao, M. M., Hallinan, G., Pineda, J. S., et al. 2016, ApJ, 818, 24
Knapp, G. R., Leggett, S. K., Fan, X., et al. 2004, AJ, 127, 3553
Koch, D. G., Borucki, W. J., Basri, G., et al. 2010, ApJ, 713, L79
Koen, C. 2013, MNRAS, 428, 2824

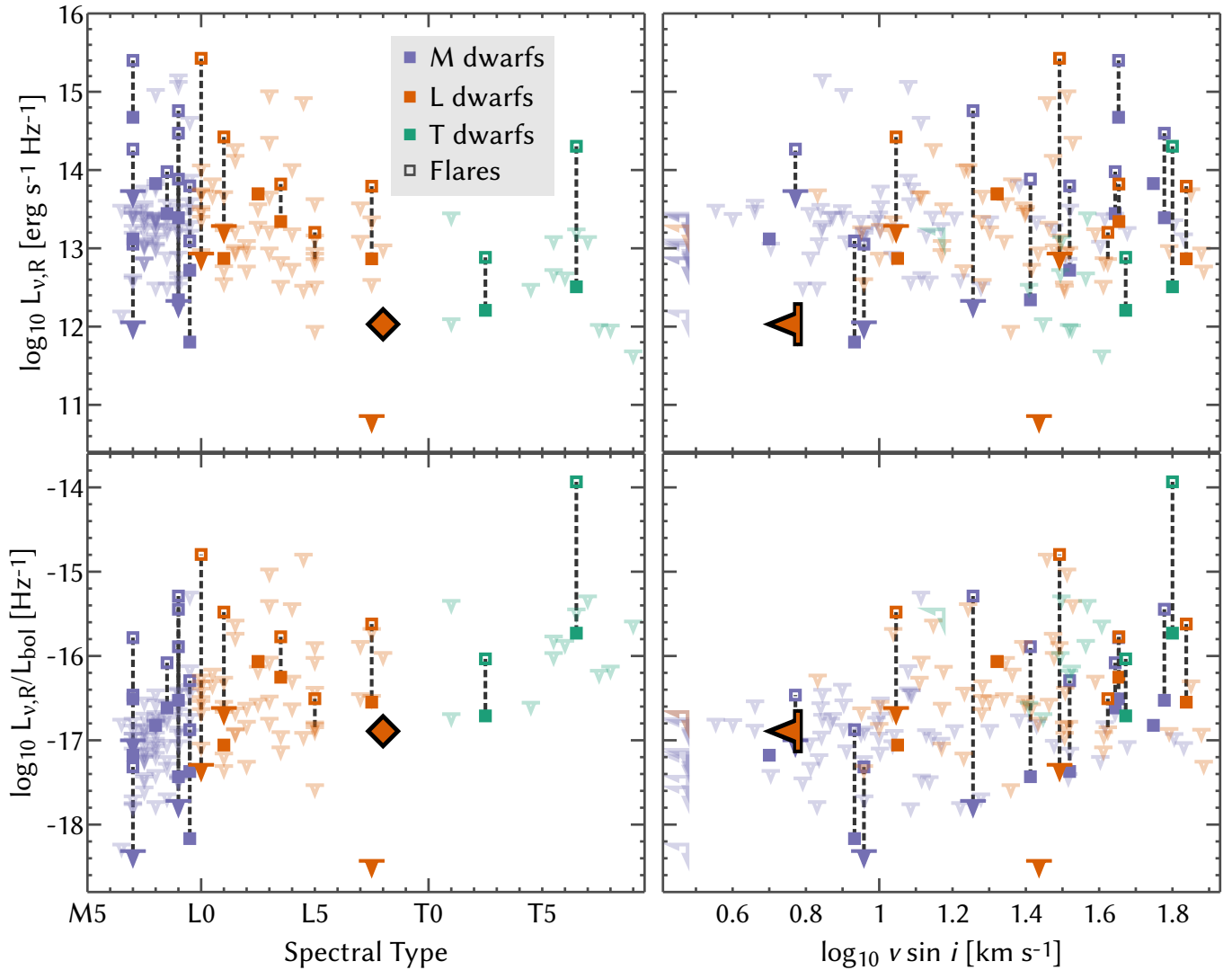**Figure 8.** Radio spectral luminosities (L_ν) of ultracool dwarfs with rotation measurements (Data from Cook et al. 2014 and references therein, Burgasser et al. 2015a, Kao et al. 2016, Lynch et al. 2016) In the lower panels these luminosities are scaled by L_{bol}. W0607+24 is highlighted with a large, black-outlined symbol. Note that while W0607+24 has a low $v \sin i$, it is not necessarily a slow rotator if $\sin i$ is small as we hypothesize. The extremely low upper limit at spectral type L7.5 is the nearby (2 pc) binary Luhman 16 AB (Osten et al. 2015). Several more late-L and T dwarfs have been detected in the radio but do not have published rotation rate measurements (Kao et al. 2016).

Libralato, M., Bedin, L. R., Nardiello, D., & Piotto, G. 2016, MNRAS, 456, 1137

Livingston, W., & Wallace, L. 1991, An atlas of the solar spectrum in the infrared from 1850 to 9000 cm-1 (1.1 to 5.4 micrometer) (National Solar Observatory)

Lynch, C., Murphy, T., Ravi, V., et al. 2016, MNRAS, 457, 1224

Martín, E. L., Cabrera, J., Martioli, E., Solano, E., & Tata, R. 2013, A&A, 555, A108

McLean, I. S., Graham, J. R., Becklin, E. E., et al. 2000, in Society of Photo-Optical Instrumentation Engineers (SPIE) Conference Series, Vol. 4008, Society of Photo-Optical Instrumentation Engineers (SPIE) Conference Series, ed. M. Iye & A. F. Moorwood, 1048

McLean, M., Berger, E., Irwin, J., Forbrich, J., & Reiners, A. 2011, ApJ, 741, 27

McLean, M., Berger, E., & Reiners, A. 2012, ApJ, 746, 23

McMullin, J. P., Waters, B., Schiebel, D., Young, W., & Golap, K. 2007, in Astronomical Society of the Pacific Conference Series, Vol. 376, Astronomical Data Analysis Software and Systems XVI, ed. R. A. Shaw, F. Hill, & D. J. Bell, 127

Metchev, S. A., Heinze, A., Apai, D., et al. 2015, ApJ, 799, 154

Mutel, R. L., Molnar, L. A., Waltman, E. B., & Ghigo, F. D. 1998, ApJ, 507, 371

Nardiello, D., Bedin, L. R., Nascimbeni, V., et al. 2015, MNRAS, 447, 3536

Offringa, A. R., de Bruyn, A. G., Biehl, M., et al. 2010, MNRAS, 405, 155

Offringa, A. R., van de Gronde, J. J., & Roerdink, J. B. T. M. 2012, A&A, 539, A95

Osten, R. A., Hawley, S. L., Bastian, T. S., & Reid, I. N. 2006, ApJ, 637, 518

Osten, R. A., Melis, C., Stelzer, B., et al. 2015, ApJ, 805, L3

Patten, B. M., Stauffer, J. R., Burrows, A., et al. 2006, ApJ, 651, 502

Perley, R. A., & Butler, B. J. 2013, ApJS, 204, 19

Radigan, J., Lafrenière, D., Jayawardhana, R., & Artigau, E. 2014, ApJ, 793, 75

Reach, W. T., Megeath, S. T., Cohen, M., et al. 2005, PASP, 117, 978

Reid, I. N., Kirkpatrick, J. D., Gizis, J. E., et al. 2000, AJ, 119, 369

Reiners, A., & Basri, G. 2008, ApJ, 684, 1390

Saumon, D., & Marley, M. S. 2008, ApJ, 689, 1327

Scholz, A., Kostov, V., Jayawardhana, R., & Mužić, K. 2015, ApJ, 809, L29

Stelzer, B., Alcalá, J., Biazzo, K., et al. 2012, A&A, 537, A94

Still, M., & Barclay, T. 2012, PyKE: Reduction and analysis of Kepler Simple Aperture Photometry data, ascl:1208.004, astrophysics Source Code Library

Tremblin, P., Amundsen, D. S., Chabrier, G., et al. 2016, ApJ, 817, L19

Treumann, R. A. 2006, A&A Rev., 13, 229

Tsuji, T., Ohnaka, K., & Aoki, W. 1999, ApJ, 520, L119

Vanderburg, A., & Johnson, J. A. 2014, PASP, 126, 948

Werner, M. W., Roellig, T. L., Low, F. J., et al. 2004, ApJS, 154, 1

Williams, P. K. G., & Berger, E. 2015, ApJ, 808, 189

Williams, P. K. G., Berger, E., Irwin, J., Berta-Thompson, Z. K., & Charbonneau, D. 2015, ApJ, 799, 192

Williams, P. K. G., Berger, E., & Zauderer, B. A. 2013, ApJ, 767, L30

Williams, P. K. G., Cook, B. A., & Berger, E. 2014, ApJ, 785, 9

Wu, C. S., & Lee, L. C. 1979, ApJ, 230, 621

Zapatero Osorio, M. R., Martín, E. L., Bouy, H., et al. 2006, ApJ, 647, 1405